Original article

Choroidal and retinal structural, cellular and vascular changes in a rat model of Type 2 diabetes

António Campos [a,b,c,d,e,1], João Martins [a,b,c,f,g,1], Elisa J. Campos [a,b,c,h,*], Rufino Silva [a,h,i], António Francisco Ambrósio [a,b,c,h,*]

[a] University of Coimbra, Coimbra Institute for Clinical and Biomedical Research (iCBR), Coimbra, Portugal
[b] University of Coimbra, Center for Innovative Biomedicine and Biotechnology (CIBB), Coimbra, Portugal
[c] Clinical Academic Center of Coimbra (CACC), Coimbra, Portugal
[d] Department of Ophthalmology, Centro Hospitalar Leiria E. P. E., Leiria, Portugal
[e] ciTechCare, Center for Innovative Care and Health Technology, Polytechnic Institute of Leiria, Leiria, Portugal
[f] University of Coimbra, Coimbra Institute for Biomedical Imaging and Translational Research (CIBIT), Coimbra, Portugal
[g] University of Coimbra, Instituto de Ciências Nucleares Aplicadas à Saúde (ICNAS), Coimbra, Portugal
[h] Association for Innovation and Biomedical Research on Light and Image (AIBILI), Coimbra, Portugal
[i] Department of Ophthalmology, Centro Hospitalar e Universitário de Coimbra (CHUC), Coimbra, Portugal

ARTICLE INFO	ABSTRACT
	Increasing evidence points to inflammation as a key factor in the pathogenesis of diabetic retinopathy (DR). Choroidal changes in diabetes have been reported and several attempts were made to validate *in vivo* choroidal thickness (CT) as a marker of retinopathy. We aimed to study choroidal and retinal changes associated with retinopathy in an animal model of spontaneous Type 2 diabetes, Goto-Kakizaki (GK) rats. Sclerochoroidal whole mounts and cryosections were prepared from 52-week-old GK and age-matched control Wistar Han rats. CT was measured by optical coherence tomography. Microglia reactivity, pericyte and endothelial cells distribution, and immunoreactivity of vascular endothelial growth factor (VEGF) and VEGF receptor 2 (VEGFR2) were evaluated by immunofluorescence. Choroidal vessels were visualized by direct perfusion with 1,1'-dioctadecyl-3,3,3',3'-tetramethylindocarbocyanine perchlorate (Dil). Choroidal vascular density was evaluated by fluorescence microscopy. GK rats had increased CT (58.40 ± 1.15 μm *versus* 50.90 ± 1.58 μm, $p < 0.001$), reduced vascular density of the choriocapillaris (CC) ($p = 0.045$), increased Iba1$^+$ cells density in the outer retina ($p = 0.003$) and increased VEGFR2 immunoreactivity in most retinal layers ($p = 0.021$ to 0.037). Choroidal microglial cells and pericytes showed polarity in their distribution, sparing the innermost choroid. This cell-free gap in the inner choroid was more pronounced in GK rats. In summary, GK rats have increased CT with decreased vascular density in the innermost choroid, increased VEGFR2 immunoreactivity in the retina and increased Iba1$^+$ cells density in the outer retina.

1. Introduction

Type 2 diabetes (T2D) accounts for more than 90 % of all cases of diabetes and is related, mostly, with age, sedentary life and diet overload [1]. Diabetic retinopathy (DR) and its complications are commonly treated with anti- vascular endothelial growth factor (VEGF) agents [2] and the greater focus has been put on the role of VEGF on the pathogenesis of DR [3,4]. VEGF-driven inner blood-retinal barrier (BRB) breakdown in the venule side of the superficial retinal vasculature has been pointed as the earliest event in DR [3] and it was related to pericyte loss and hypoxemia [5]. Nevertheless, VEGF is not increased in the vitreous of all patients with diabetic macular edema (DME), while proinflammatory markers were found to be increased [6]. Accordingly, about one third of patients with DME fail to respond to anti-VEGF therapy [7]. Those facts pointed DR to be an inflammatory condition and that was confirmed experimentally [8,9]. The retinal resident innate immune system, which is primarily composed of tissue-resident macrophage-like microglial cells, become activated and start to produce proinflammatory mediators [9]. The perspective of DR as an inflammatory disease brought new attention on previous works describing choroidal inflammatory alterations in diabetes, named as 'diabetic choroidopathy', including Bruch's membrane deposits and increased thickness, and choriocapillaris (CC) dropout [10,11]. Since the advent of optical coherence tomography (OCT), the choroidal thickness (CT) has been sought as a surrogate of choroidal flux, diabetic choroidopathy or DR, but the results are conflicting and disappointing [12–15,20]. Recent works did not unveil the contradictions. The CT was found to be decreased [16–21], increased [15,22], or unchanged [14,23] in T2D patients. More recently, it was reported that the CT increased in the early stages of DR, and further decreased with DR progression [24]. The thinning of the choroid with the anti-VEGF treatment of DME increased the assumption that the choroid thickens in DR and DME in an VEGF-dependent exclusive manner [13]. Nevertheless, the thinning of the choroid under anti-VEGF treatment seems to be only a side effect, with poor prognostic value [25], focusing back the attention on cellular and molecular signatures that might take place in diabetic choroidopathy. Indeed, the water homeostasis in the retina and in the choroid depend on different cell types. Retinal water clearance at the choroid level depends on the oncotic pressure underneath the retinal pigment epithelium (RPE), developed by the existence of VEGF-dependent pores in the CC [26]. However, anti-VEGFs were found to decrease such pore number [27]. The thickening-back of the choroid in DME, when the anti-VEGF effect subsides, may not necessarily be related to the water homeostasis in the retina, but to reversible vasoconstriction [28,29].

Several animal species, mostly rodents, have been used as validated models for diabetes and to study the cellular and molecular aspects of the pathogenesis of DR [30,31]. Animal models of T2D include: i) obese animal models, such as Lep$^{ob/ob}$ mice, Lepr$^{db/db}$ mice, Zucker diabetic fatty rats, Otsuka long-Evans Tokushima fat (OLETF) rats [31], as well as high fat feeding [32]; and ii) nonobese animal models, such as Goto-Kakizaki (GK) rats and spontaneously diabetic Torii (SDT) rats [30, 31]. The GK rats are one of the most useful animal models for studying the pathophysiologic progress of T2D and its complications, namely retinopathy, as formerly published articles in our institute showed [33, 34]. GK rats are a lean model of T2D, which is characterized by early and relatively stable mild hyperglycemia, hyperinsulinemia, and insulin resistance [31]. Moderate diabetic condition allows for prolonged disease in GK rats, similarly to what is observed in humans. GK rats also present some features found in patients with DR and thus they are a model to study the kinetics and events of T2D. Increased NO production, early inner BRB breakdown and migration of activated microglial cells from the retina to the choroid by transcytosis has been demonstrated in GK rats [34–36], but the breakdown of the outer BRB and Bruch's membrane permeability in diabetes is not completely understood yet [37].

We investigated the impact of T2D on the CT and choroidal vascular density, as well as on endothelial cells and pericytes, microglial cell reactivity, VEGF and VEGF-receptor 2 (VEGFR2) immunoreactivity, in the retina and choroid of GK (52 weeks old, 52 W) and age-matched control Wistar Han rats.

2. Materials and methods

2.1. Animals

Male spontaneously diabetic GK rats were obtained from the Faculty of Medicine of University of Coimbra breeding colony established in 1995 with breeding couples from the colony at the Tohoku University school of Medicine (Sendai, Japan; courtesy of Dr. K. I. Susuki). Control animals were age-matched non-diabetic male Wistar rats, obtained from our local colony at the Coimbra Institute for Clinical and Biomedical Research (iCBR). Animals were housed in the certified animal facility at iCBR, on a 12 h light/12 h dark cycle, at 22−23 °C, and 60 % relative humidity, and with free access to water and to rodent standard maintenance chow (4RF21, Mucedola s.r.l., Settimo Milanese, Italy) containing 18.5 % of protein and 3.0 % of lipids. Animals further got shredded paper and cardboard rolls for nest building and shelter. All procedures were approved by the Animal Welfare Committee of the Coimbra Institute for Clinical and Biomedical Research (iCBR), Faculty of Medicine, University of Coimbra. The animals received humane care according to the criteria outlined in the Guide for the Care and the Use of Laboratory Animals prepared by EU Directive 2010/63/EU for animal experiments and with the Association for Research in Vision and Ophthalmology (ARVO) statement for animal use. At 52 W, the animals (n = 12, control group; n = 16, GK group) were weighted and glycemia was measured using a glucometer (Ascensia ELITE™, Bayer Corporation, Mishawaka, IN, USA).

2.2. Optical coherence tomography

The animals were anesthetized *via* i.p. injection with ketamine 80 mg/kg + xylazine 5 mg/kg (80:5, for short; Imalgene 1000, Merial, Lyon, France, and Rompum®, Bayer, Leverkusen, Germany, respectively), and cornea anesthesia (4 mg/mL oxybuprocaine hydrochloride; Anestocil®, Laboratório Edol, Carnaxide, Portugal), pupils dilation (1 %, Tropicil®, Laboratório Edol, Carnaxide, Portugal) and corneal hydration (2 % Methocel™, Dávi II Farmacêutica S.A., Barcarena, Portugal) was kept during procedure.

The CT was evaluated in the animals using spectral domain optical coherence tomography (SD-OCT) at 52 W. The SD-OCT system is able to capture 10,000–20,000 A scans per second with an axial resolution of 2 μm and a transverse resolution of 4 μm. OCT was performed in both eyes of all animals at 52 W, just before being euthanized. The 830 nm SD-OCT Imagine System (Phoenix Micron IV, Phoenix Research Labs, Pleasanton, CA, USA) [38] was placed closer to the eye such that an inverted image was obtained and the deeper structures were placed closer to zero-delay [39]. Scans were obtained superior to the optic nerve head/optic disc (ONH), in both eyes of all animals, in the area within 1–3 ONH diameter from the optic disc. For each location, the device collected a set of 1024 raster scans along the scan length. Upon collection, a set of five images was converted into a single image to reduce the noise observed on individual images. The CT was measured using InSight image segmentation software (v.1, Voxeleron LLC - Image analysis solutions, Chabot Drive, CA, USA). An average of three independent scores obtained from 3 sets "five frames averaged" was used as the CT value *per* eye *per* time-point.

2.3. Tissue preparation for cryosections

The animals were anesthetized, as described above, and intracardially perfused with 0.1 M phosphate buffer saline (PBS, 137 mM NaCl, 2.7 mM KCl, 1.8 mM KH$_2$PO$_4$, 10 mM Na$_2$HPO$_4$, pH 7.4), followed by 4 %

paraformaldehyde (PFA) in 0.1 M PBS, pre-warmed at 37 °C.

The enucleated eyes of GK (n = 8) and age-matched control Wistar Han (n = 5) rats were post-fixed in 4% PFA for 1 h. The eyes were washed in successive solutions of PBS and immersed in solutions containing 15 % and 30 % of sucrose in PBS, for 1 h in each solution. They were embedded in a 1:1 30 % sucrose and embedding resin (Shandon™ Cryomatrix™, Thermo Fisher Scientific, Waltham, MA, USA) solution, before freezing in dry ice. The samples were stored at -80 °C, until further use. Eyeball sections 14 μm-thick from both right and left eyes were obtained using a cryostat (Leica CM3050S, Nussloch, Germany), at -22 °C, and mounted on adhesive slides (Superfrost Plus™, Thermo Fisher Scientific). A total of four sections (14 μm apart) were collected *per* slide.

2.4. Immunofluorescence

Eye sections were labeled to assess the retinal and choroidal structure, following a procedure described previously [40]. The cryosections were rehydrated twice in PBS for 5 min, followed by blocking and permeabilization for 1 h in 10 % goat serum and 0.5 % Triton X-100 in PBS. The sections were then incubated overnight with primary antibodies (Table S1) diluted in 0.5 % Triton X-100, at 4 °C. After washing with PBS, sections were incubated with corresponding secondary antibodies (Table S2) diluted in 0.5 % Triton X-100, for 1 h. After washing, the sections were incubated with 1:5,000 4',6-diamidino-2-phenylindole (DAPI, Invitrogen™), and coverslipped using mounting medium (Glycergel, Dako, Carpinteria, CA, USA).

Digital images were captured using an inverted fluorescence microscope (Axio Observer.Z1, Zeiss, Carl Zeiss Meditec AG, Jena, Germany) and a laser scanning confocal inverted microscope (LSM 710 Axio Observer, Zeiss), using objectives "Plan-Apochromat" 20×/0.8 (Zeiss).

Eight bit images were analyzed using the ImageJ software (version 1.48, National Institutes of Health, USA) [41]. Iba1$^+$ and MHC II$^+$ cells were manually counted in the choroid and retina. Data were expressed as number of cell/mm of choroidal or retinal length, respectively. Rat endothelial cell antigen 1 (RECA-1) and the neural-glial antigen 2 (NG2) immunoreactivities were scored in the choroid as fluorescence intensity *per* area selected (reference area selected of $10,737.08 \pm 6,306.11$ μm^2), while fluorescent NG2$^+$ cells and RECA-1 focal immunostaining were manually counted in the retina. VEGF and VEGFR2 immunoreactivity was quantified as fluorescence intensity/area for each layer analyzed. All results were expressed as the mean count of 12 slices *per* eye (right eye only).

2.5. Direct labeling and visualization of choroidal vessels in sclerochoroidal whole mounts

Intracardiac perfusion with PBS was performed in rats (n = 7, control group; n = 8, GK group) under anesthesia (i.p.; ketamine:xylazine 160:30). DiI (Cat. #D-282, Invitrogen™, Carlsbad, CA, USA) 0.120 mg/mL in 1 % glucose in PBS was applied *via* cardiac perfusion, following perfusion with 4 % PFA. The eyes were enucleated, and choroidoscleral whole mounts were prepared. The whole mounts were fixed in 4 % PFA for 15 min, washed with PBS, and blocked with 10 % goat serum in 0.3 % Tween in PBS for 1 h. Samples were incubated with the primary antibodies diluted in 3 % goat serum in PBS for 3 days at 4 °C (Table S1). After washing overnight with PBS, whole mounts were incubated with secondary antibodies (Table S2) overnight at 4 °C. After washing, samples were flat mounted onto glass slides using mounting medium. The images were obtained by laser scanning confocal microscope LSM 710 (Zeiss), using an objective EC "Plan-Neofluor" 40×/1.30 Oil M27 (Zeiss). A series of z-stacks were captured from the RPE outer surface, to the outer choroid. Each z-stack consisted of a depth of optical sections, 3 μm apart, along the z-axis. Iba1$^+$ and MHC II$^+$ cells were classified as ramified or round cells and were manually counted in the choroid in all in-depth planes of the slide (Fig. S1). The choroidal vascular density

(defined as the percentage of total area covered by CC vessels) [42] was determined from independent z-stacks collected at ≤ 10 μm (CC) and > 10 μm outwards from the RPE plane (medium and large vessels) in a selected area (213 × 213 μm, Fig. S2). Results were expressed as the mean of 14 counts per eye.

2.6. Statistical analysis

The statistical analysis was performed using SPSS (Version 25.0, IBM Corp., Armonk, NY, USA). The Shapiro-Wilk test was used to assess the normality of data ($p > 0.05$). The normally distributed data were evaluated concerning the homogeneity of variance, using the Levene's test ($p > 0.05$). The independent *t*-test was used to compare the means between two experimental groups for the same variable. Statistical significance was defined as $p < 0.05$. Values were presented as mean ± standard error of the mean (SEM).

3. Results

3.1. Diabetic animals exhibit decreased body weight and hyperglycemia

A total of 28 animals (52 W) were enrolled in the study (16 GK and 12 age-matched control Wistar Han rats). The weight of GK rats was significantly lower than that of age-matched control rats (416.31 ± 7.0 g and 462.5 ± 9.24 g, respectively, $p < 0.001$) and glycemia was significantly higher (227.75 ± 12.1 mg/dL *versus* 107.0 ± 0.94 mg/dL, $p < 0.001$, Fig. S3).

3.2. Increased choroidal thickness in GK rats

CT was assessed in both eyes of all GK (n = 32 eyes) and age-matched control Wistar Han (n = 24 eyes) rats at 52 W, using OCT. CT was higher in GK rats (58.40 ± 1.15 μm *versus* 50.90 ± 1.58 μm, $p < 0.001$, Fig. 1A and B).

3.3. Choroidal blood vascular density is reduced in the inner choroid in GK rats

Fifteen animals (8 GK and 7 age-matched control Wistar Han rats) were assigned to perfusion with DiI and sclerochoroidal whole mounts were prepared and assessed by confocal microscopy.

The choroidal vascular density in the innermost choroid/ CC (≤ 10 μm) was significantly decreased in GK rats ($p = 0.045$, Fig. 2A and C and Table S3). Choroidal Iba1$^+$ and MHC II$^+$ cell number was not significantly different between GK and age-matched control rats (Fig. 2B and D and Table S4).

Interestingly, Iba1$^+$ cells and MHC II$^+$ cells topographic disposition in the choroid spare the innermost choroid, where they are notably rare or absent, being preferentially present in the middle and outer choroidal stroma, either in GK or age-matched control rats (Videos S1-6).

3.4. Increased immunoreactivity of microglial cell markers in the outer retina of GK rats

Iba1$^+$ cells increased in the retina of GK rats, being statistically significantly increased in the outer plexiform layer (OPL, $t(11.000) = -3.872$, $p = 0.003$). Iba1$^+$ ($p = 0.195$) and MHC II$^+$ cells density was not statistically significantly different in the choroid of GK rats ($t(11.000) = 2.190$, $p = 0.051$, Fig. 3 and Table S5). Interestingly, Iba1$^+$ cells were distributed throughout the retina of GK rats paralleling the topographic distribution of the 3 vascular plexuses of the retina. Iba1$^+$ cell extensions from the inner plexiform layer (IPL) to the OPL resemble the communications between the deep and middle vascular plexuses of the retina, suggesting that migrating glial cells towards the outer retina may use the communicating inter-plexuses retinal capillaries as a scaffold (see Fig. 3A, bottom left panel). Communications between plexus were

A

Control   GK
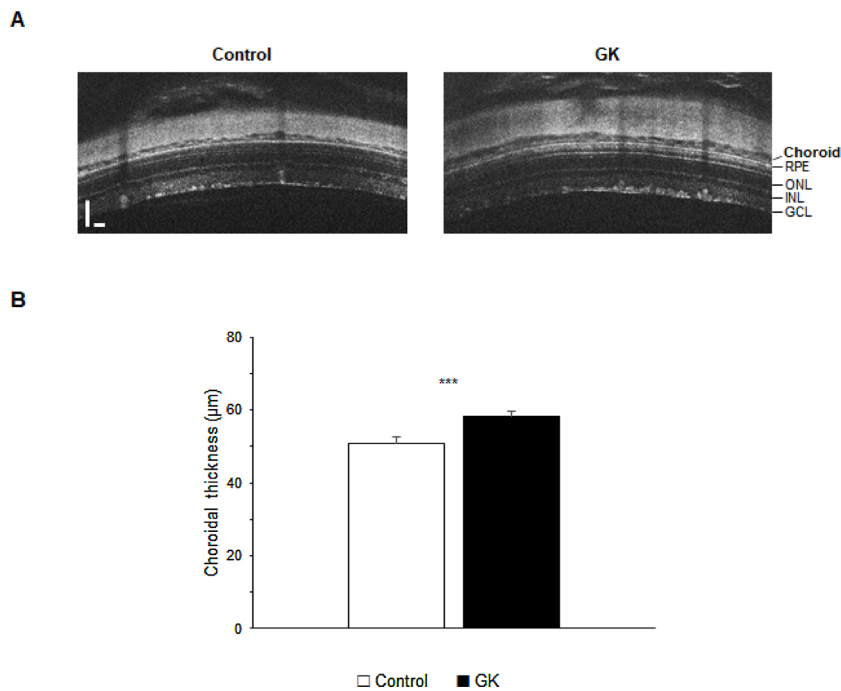
Choroid
RPE
ONL
INL
GCL

B

Fig. 1. Choroidal thickness (CT) of GK and age-matched control Wistar Han rats (52 W). (A) Images resulting from five frames averaged, collected as inverted images using OCT raster scans obtained in 1024 continuous points, by approaching the device to the zero delay line. Horizontal raster scan line encompasses an area within 1 to 3 disc diameters from the optic nerve head. Choroidal layer obtained by automatic segmentation was manually corrected. A mean of three independent scores obtained from 3 different located sets "five frames averaged" were used as the CT value *per* eye *per* time-point. (B) CT values from all eyes of GK (n = 32) and age-matched control (n = 24) rats. Data are expressed as mean ± SEM. Scale bar: 100 μm. Significance between groups was determined using the independent *t*-test: ***$p < 0.001$. GCL, ganglion cell layer; INL, inner nuclear layer; ONL, outer nuclear layer; RPE, retinal pigment epithelium.

evidenced.

3.5. Pericytes are rare in the innermost choroid of GK rats

There were no statistically significant differences in the immunoreactivity of NG2 and RECA-1 between GK and age-matched control Wistar Han rats, whatever the location considered (Fig. 4 and Table S6). Nevertheless, there was a trend to increased NG2 immunostaining in the choroid of GK rats. Combined immunoreactivity of RECA-1 and NG2 evidenced a rarefaction of pericytes in the innermost choroid of GK rats. RECA-1 co-localized with the CC layer, just underneath and in close continuity with the RPE cell plane (Fig. 4A, left panels). NG2 immunoreactivity was absent in some areas of the CC plane, leaving fluorescent-free gaps between the RPE and the inner choroid, drawing a typical jagged pattern, corresponding to the absence of pericytes/mural cells in the innermost choroid (Fig. 4A, middle panels, blue arrows). This 'polarity' in choroidal vascular regulatory cells disposition evidenced by NG2, corresponding to a rarefaction of pericytes in the innermost choroid, was more evidenced in GK rats. The three retinal plexuses (superficial, in the retinal nerve fiber and ganglion cell (GCL) layers; middle, in the IPL and deep, in the OPL) were visualized by RECA-1 immunolabeling (Fig. 4A, top panels, left and right).

3.6. VEGFR2 immunoreactivity was significantly increased in GK rats

VEGF immunoreactivity was more intense in the level of the OLM, RPE and choroid, while VEGFR2 immunoreactivity was negligible at those locations. VEGFR2 immunoreactivity was more intense in the inner retina. Higher VEGFR2 immunoreactivity was observed in GK rats, significantly in the IPL, INL, OPL, ONL and OLM, when comparing with age-matched control rats (Fig. 5 and Table S7).

4. Discussion

CT has been searched as a surrogate of DR, DME, choroidal flux and diabetic choroidopathy in T2D patients, but contradictory results have been reported [12–15,20]. Although GK rats are not blueprints for the diseased T2D humans, they provide excellent insights into the pathogenesis of T2D [43]. Furthermore, rats are recognized as the preeminent

model for studying the choroid [44,45]. We found that CT was significantly increased in GK rats when comparing with age-matched control Wistar Han rats. To our knowledge, this is the first time that the CT is assessed *in vivo* in a rat model of T2D.

The vascular density was reduced in the inner choroid of GK rats, corresponding to the CC. This observation is in accordance with CC degeneration observed in T2D humans, either by postmortem specimens or by OCT-angiography (OCTA) [11,46]. OCTA binarization technique in human diabetics showed results of decreased flow or depletion at the CC level that agree with our results in the animal [47]. The findings of no significant difference in the outer choroid's vascular density combined with a significantly higher CT in GK rats, enhances the role of the outer choroid layer, the suprachoroid, as an important contributor to total CT and may explain why available data on human CT are so contradictory [13–15,48,49]. The suprachoroid is the choroidal layer most prone to change, but it is the most difficult to evaluate correctly when not using high definition devices such as the Swept Source OCT and the high resolution mode enhanced deep imaging (EDI) of the SD-Spectralis OCT [12,25]. Unfortunately, devices based on red blood cells' movement as the OCTA are not expected to help much in this issue either [50].

The normal distribution of inflammatory cells in the choroidal stroma, sparing the innermost choroid, suggests that under inflammatory stress a dramatic increase in the number of inflammatory cells may result in packing of cells at this area, leading to disturbances of the photoreceptors/RPE/Bruch's membrane/CC tapetoretinal unit (S1-3 Videos) [51]. Nevertheless, we did not find inflammatory cells to be significantly increased in the choroid of GK rats. It is possible that this finding correlates with the low level of diabetes in this animal model. Actually, we found increased inflammatory cells in the choroid of a more aggressive diabetic animal model, streptozotocin-induced Type 1 diabetes (T1D) [52]. The number of inflammatory cells were increased in the retina, as previously described, mainly in the OPL [9,36]. Interestingly, Iba1$^+$ cells disposition parallels the three retinal plexuses', and the migration of cells from the inner to the outer retina resembles the capillary communications between plexuses, suggesting that vessels are a scaffold for cell migration.

The VEGF levels were not significantly increased in the retina, RPE or choroid, in GK rats. VEGFR2 expression was negligible in the RPE or choroid both in GK and age-matched control Wistar Han rats.
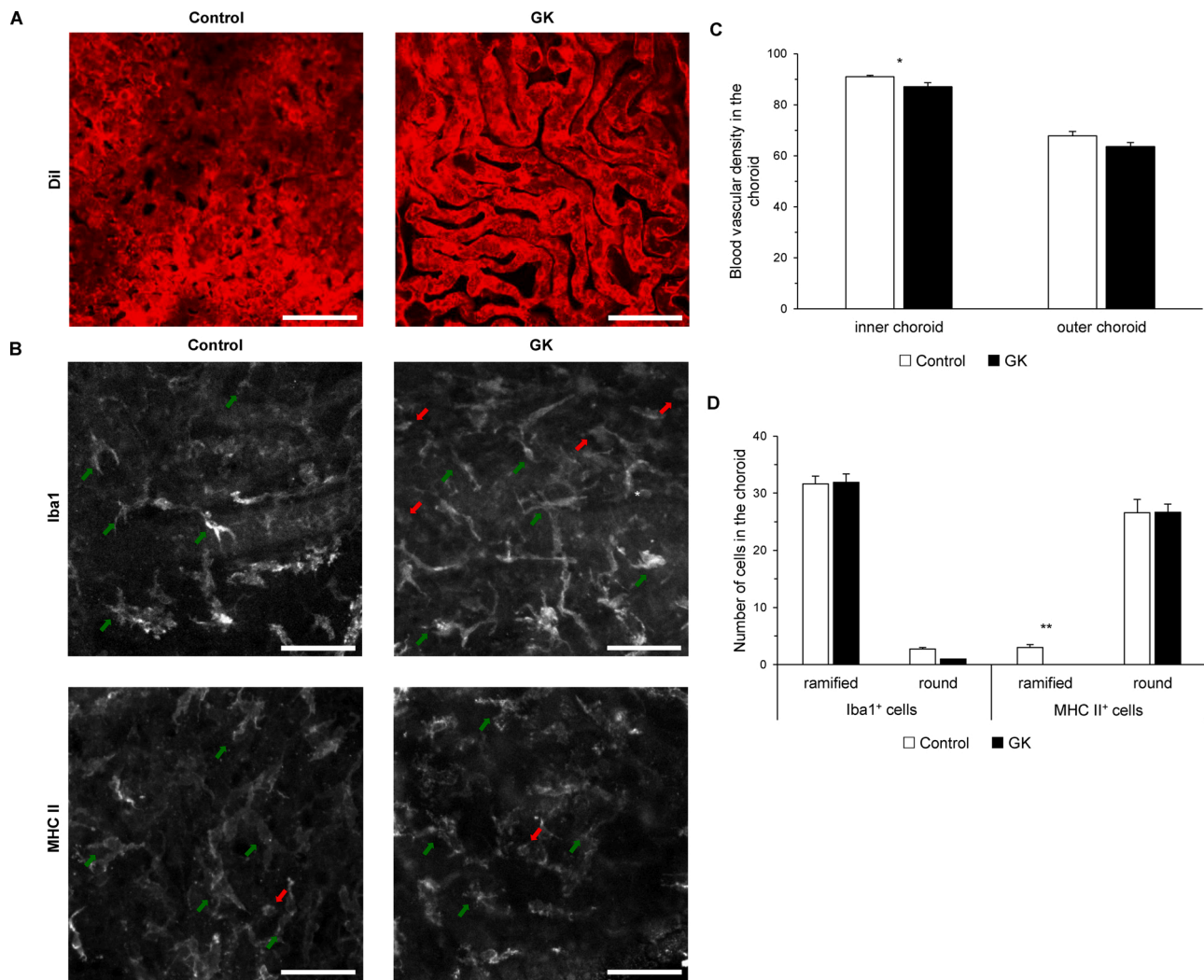
Fig. 2. Vascular and cell profiles of the choroid of GK and age-matched control Wistar Han rats (52 W). (A) Representative images of vascular density in the inner choroid (≤ 10 µm). **(B)** Choroidal Iba1$^+$ and MHC II$^+$ cells. Ramified cells (green arrows) and round cells (red arrows) were highlighted. **(C)** Quantification of the choroidal vascular density in the inner and outer choroid using the 'image > adjust > threshold' window tool of ImageJ to obtain the percentage of vascular coverage, obtained from z-stacks collected at ≤ 10 µm or > 10 µm from the outer RPE plane, respectively. **(D)** Iba1$^+$ and MHC II$^+$ cell number in the choroid in all in-depth z-stacks. Images were collected with Zeiss EC Plan-Neofluor 40x oil objective lens, NA 1.3. Quantitative analyses were performed based on 14 independent counts *per* eye in each and all in-depth z-stacks *per* specimen. Data are expressed as mean $\pm$ SEM (n = 7, control group; n = 8, GK group). Scale bar: 50 µm. Significance between groups was determined using the independent *t*-test: *$p < 0.05$, **$p < 0.01$. (For interpretation of the references to color in this figure legend, the reader is referred to the web version of this article).

Conversely, VEGFR2 immunoreactivity peaked in the retinal nerve fiber layer of both GK and control rats, and it was increased throughout the retina of GK rats. The precise cellular background for this increased expression is not clear, but the combination of maximum expression in the innermost retina and expression throughout the retina resembles the distribution of Müller cells and neurons within the retina. Nevertheless, a previous report in an animal model of T1D showed VEGFR2 to be expressed mainly in the capillaries of the retina and, in opposition to our findings, in the CC [53]. Conversely, other data correlated VEGFR2 more strikingly with neurons and Müller cells rather than with endothelial cells [54]. Interestingly, the VEGFR2 expression by neurons and Müller cells combined with the action of MHC II$^+$ cells, was related with capillary vertical sprouting and the formation of the deep retinal plexus, an example of neurovascular crosstalk or coupling. The relationship between increased VEGFR2 and normal VEGF immunoreactivity is not clear, if any at all. If that results from a milder diabetes in our model, VEGFR2 would be among the first molecular biomarkers to change in DR. However, this datum needs to be confirmed in future studies.

Disposition of pericytes in the CC was previously described in mice to

be at its scleral side only (polarized distribution) and focal pericyte depletion has been related to vascular remodeling [55]. We found distribution of NG2$^+$ cells in the innermost choroid to draw a jagged pattern, when comparing with RECA-1 endothelial immunostaining. These focal 'gaps', suggesting the existing of cell-free spaces in the innermost choroid, may be related to vascular remodeling of the CC and not necessarily to permanent alterations, and were more pronounced in T2D. Interestingly, this disposition is shared by stromal Iba1$^+$ cells in the same location (S1−6 Videos). Reduction of the vascular component of the diabetic CC reported in OCTA studies did not separate permanent degenerative from transient and reversible changes, mirroring increased CC remodeling in diabetes reported in postmortem studies in humans and in rats [11,49,50,56]. Increased remodeling of the CC, probably mediated by abluminal pericytes contacting the endothelium as peg-in-socket or tongue-in-socket processes, may be an adaptation to the pore kinetics, water load, ionic and pH alterations, VEGF levels and the presence of inflammatory mediators and cells in the diabetic choroid [55,57]. OCTA, being able to resolve the microvascular network of the retina and nonperfusion areas at the CC, does not evaluate hitherto
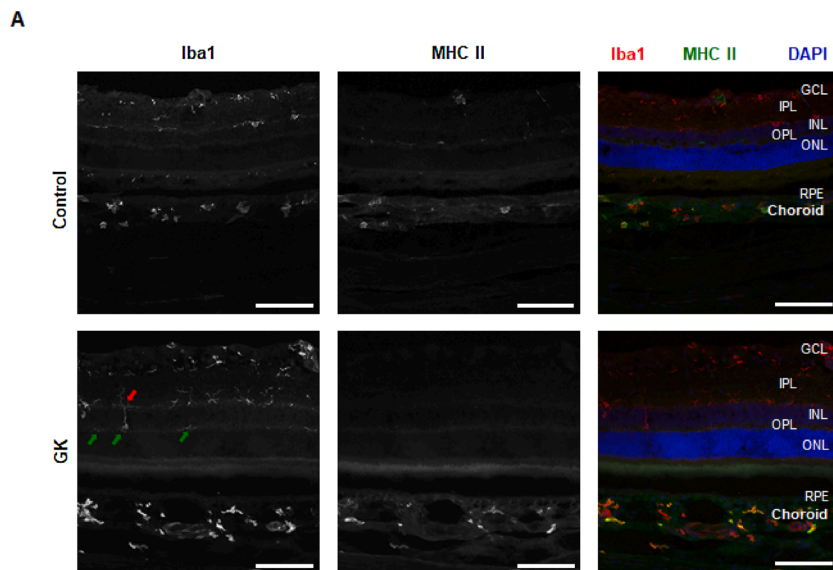
A

Fig. 3. Microglial cells in the retina and choroid of GK and age-matched control Wistar Han rats (52 W). (A) Representative eye cross-sections immunolabeled against Iba1 (left panels), MHC II (middle panels) and merge (right panels). Iba1$^+$ cells are located in the superficial and plexiform layers of the retina, mainly. Iba1$^+$ cells located in the OPL of the GK cohort only (green arrows). In GK rats, Iba1$^+$ cells migrate from the IPL to the OPL, crossing the INL (red arrow). **(B)** Quantification of Iba1$^+$ and MHC II$^+$ cell density of GK (n = 8) and age-matched control (n = 5) rats based on 12 independent specimen counts *per* eye. Counting was done for the right eye only, in all animals. Data are expressed as mean ± SEM. Scale bar: 100 μm. Significance between groups was determined using the independent *t*-test: **$p < 0.01$. GCL, ganglion cell layer; IPL, inner plexiform layer; INL, inner nuclear layer; OPL, outer plexiform layer; ONL, outer nuclear layer; RPE, retinal pigment epithelium. (For interpretation of the references to color in this figure legend, the reader is referred to the web version of this article).

B
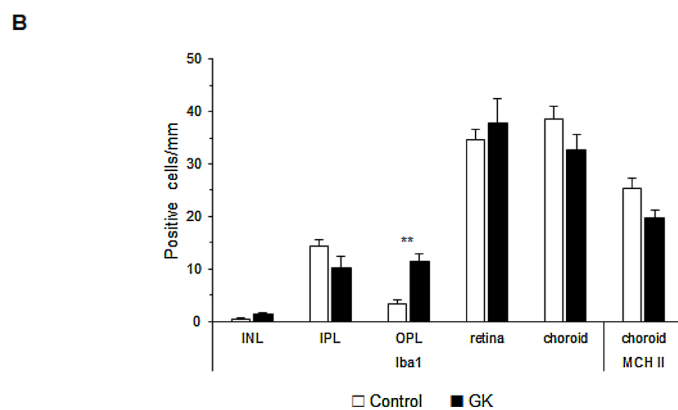
detailed morphological vascular patterns of the CC, since being as thin as 10−20 μm, it is not resolved by a system that has a maximum lateral resolution within that range (~15−20 μm), [58] and, as aforementioned, it is not suitable to evaluated the whole CT.

Increased choroidal thickness in GK rats might be related to water homeostasis and regulation of the extracellular fluid, since the choroidal vascular flux has been reported to decrease in diabetes [59,60]. This issue is not completed understood yet, but as the water pathway across the retina follows a direction from the vitreous to the choroid, one may assume that increased VEGF levels and increased capillary permeability in the retina, may increase the extracellular fluid in the retina increasing the water load on the choroid *via* a well-functioning RPE [38]. Choroidal-dependent retinal drying is modulated by pore regulation of the CC, which are mainly facing the RPE side of the CC and are VEGF-dependent [57,61]. This water overload is very well pictured in OCT when there is impairment of the RPE in DME and subretinal fluid accumulates, as a consequence of impairment of the active ionic transport by the RPE [62]. This may explain in part why the choroid thins with anti-VEGF administration by intravitreal injections, as a consequence of improved inner BRB homeostasis and decreased water load on the choroid [25]. This retina-centered line of thought may be enforced by realizing that under anti-VEGF administration pore distribution in the CC is reduced, thus decreasing the choroidal-dependent retinal drying mechanism [27]. Moreover, the restoration of active ionic transport by the RPE, with resolution of subretinal fluid *via* water flow into the choroid, would be expected to thicken and not to thin the

choroid, as actually happens [62].

A most likely explanation for CT decrease with anti-VEGFs is a reversible vasoconstriction of the choroidal vessels, as demonstrated in the retinal vessels [28,29], under pericyte regulation [55,63]. In the choroid, the blood flows in arteries and veins in the same direction, contrariwise to most organs. It is possible that some regulation of this vascular pathway, namely by pericytes or inflammatory cells, from the short posterior ciliary arteries to the vortex veins occurs at different levels, including the CC [64]. Perivascular mural cells in the middle and outer choroid were previously reported to show contractile properties that were related to vasoregulatory functions [55]. Moreover, pericyte loss has been reported in GK rats [65], mediated by hypoxia and/or inflammation, *via* vascular endothelial receptor 1 (VEGFR1, Flt-1), nitric oxide (NO) and reactive oxygen species (ROS) [63].

In addition, VEGF interacts with several vasoactive agents. NO plays a critical role in many VEGF actions [66]. Endothelial nitric oxide synthase (eNOS), which is expressed in the CC, regulates the choroidal vasculature, since production of NO by this enzyme, causes vasodilation [57]. Since there are no true lymphatic vessels in the choroid, a significant amount of extracellular fluid is reabsorbed *via* the lamellae of the suprachoroid that are under non-vascular smooth muscle cells regulation and are responsive to multiple inflammatory cytokines [12]. Increased NO may be involved in decreased extracellular fluid reabsorption in the suprachoroid. Apart from vasodilation, NO induces increased permeability of pre-terminal choroidal arteries or post-capillaries veins, as well [66], despite the reduction of choroidal
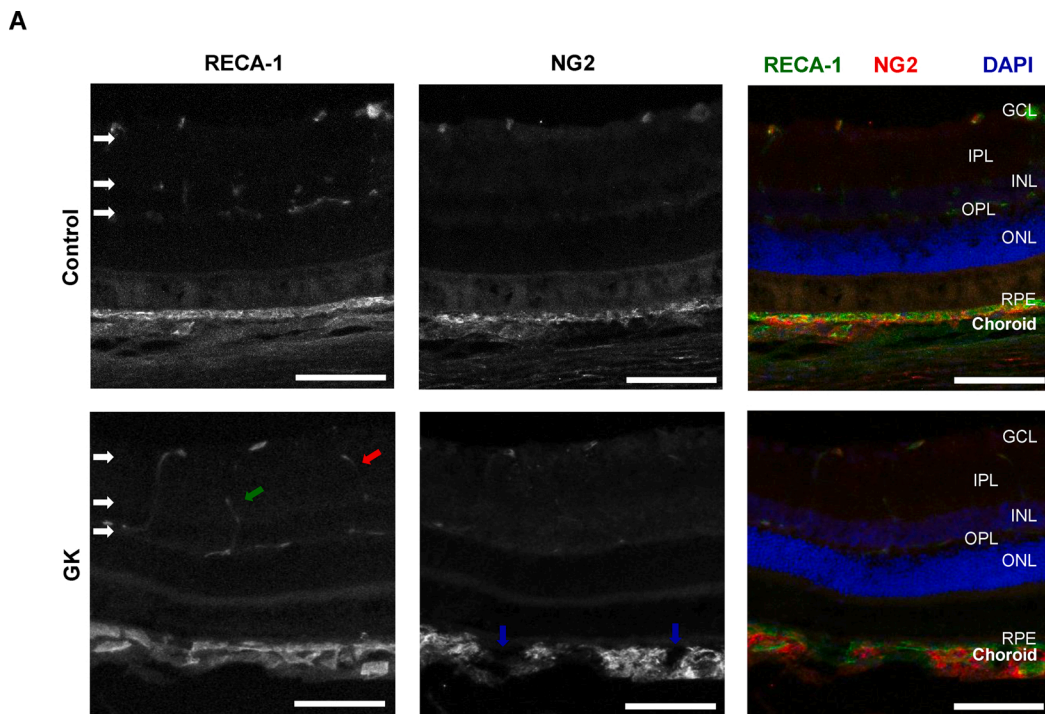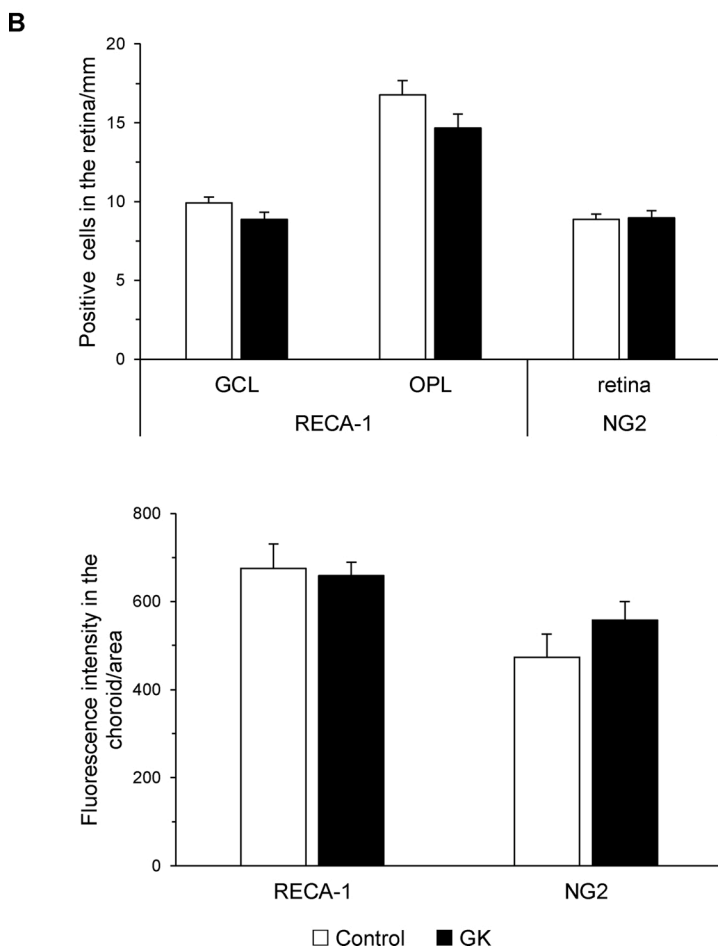
Fig. 4. Localization of mural and endothelial cells in the retina and choroid of GK and age-matched control Wistar Han rats (52 W). **(A)** Representative eye cross-sections immunolabeled against RECA-1 (left panels), NG2 (middle panels) and merge (right panels). The 3 plexuses of the retina are evidenced by RECA-1 immunostaining (white arrows). Communications between (*i*) the superficial and middle plexuses of the retina (red arrow), (*ii*) the middle and deep plexuses and (*iii*) the deep and superficial plexuses (green arrow), are visible. RECA-1 immunoreactivity relates to the presence of endothelial cells and fluorescence of the CC endothelial cells is continuous with the RPE cell plane (left panels). Conversely, NG2 immunostaining of pericyte/mural cells leaves focal gaps between the RPE and the inner choroid, drawing a jagged pattern, more pronounced in GK rats (blue arrows). **(B)** Quantification of RECA-1 and NG2 immunoreactivity in the retina and choroid of GK (n = 8) and age-matched control (n = 5) rats. RECA-1 and NG2 immunoreactivities were scored as fluorescence intensity per area selected in the choroid (reference area selected of 10,737.08 ± 6,306.11 μm^2), while NG2$^+$ cells and RECA-1 focal immunostaining were manually counted in the retina. Counting was done for the right eye only, in 12 independent specimen counts *per* eye. Data are expressed as mean ± SEM. Scale bar: 100 μm. GCL, ganglion cell layer; IPL, inner plexiform layer; INL, inner nuclear layer; OPL, outer plexiform layer; ONL, outer nuclear layer; RPE, retinal pigment epithelium. (For interpretation of the references to color in this figure legend, the reader is referred to the web version of this article).
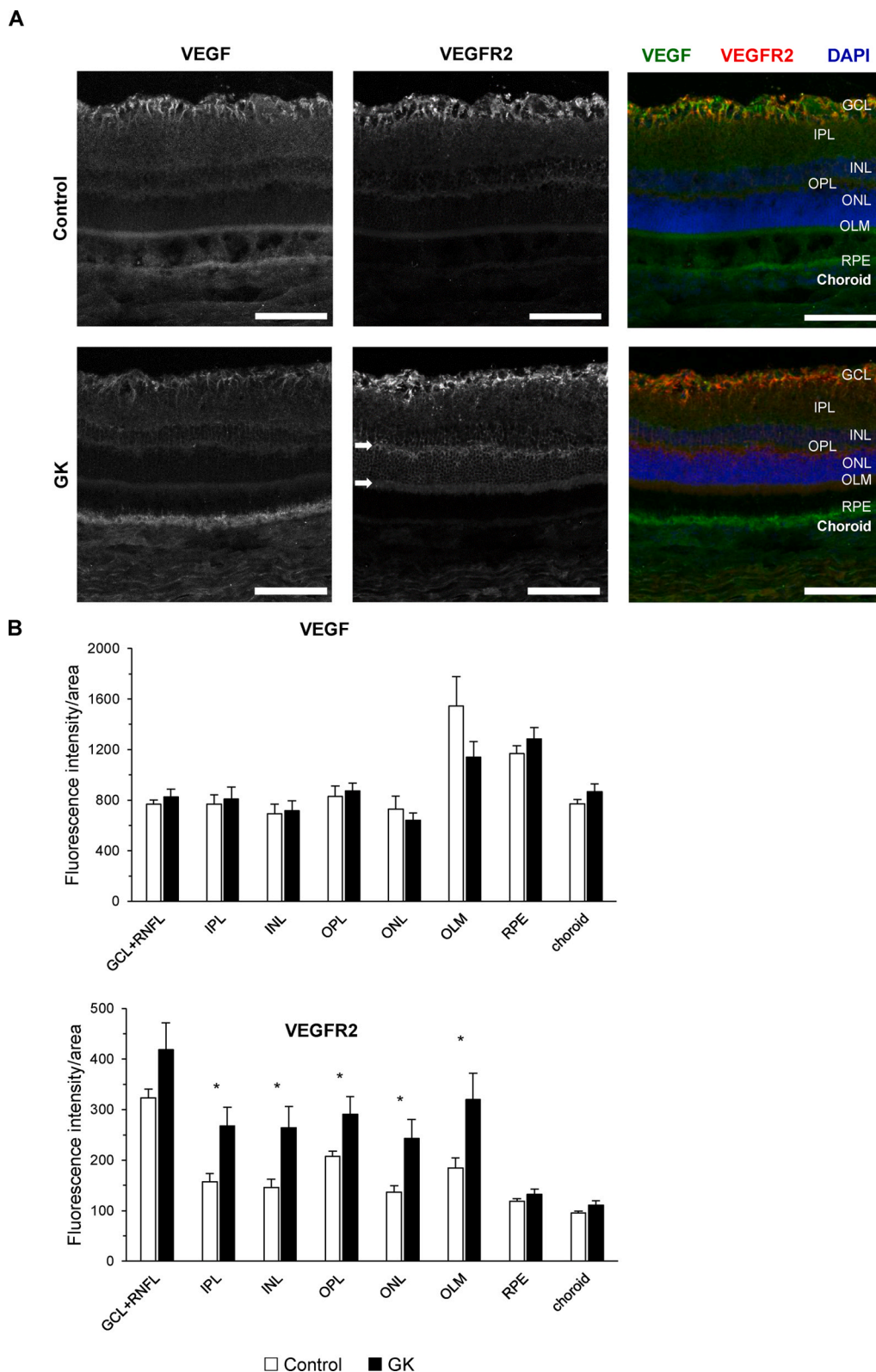
Fig. 5. Immunoreactivity of VEGF and VEGFR2 of GK and age-matched control Wistar Han rats (52 W). (A) Representative eye cross-sections immunolabeled against VEGF (left panels), VEGFR2 (middle panels) and merge (right panels). VEGF immunoreactivity spreads throughout the retina, increasing in the OPL, OLM, RPE and choroid. VEGFR2 immunoreactivity is higher in the innermost retina (retinal nerve fiber layer) and very low or absent in the RPE and choroid. VEGFR2 immunoreactivity is still visible as a faint coloration in the retinal layers other than the retinal nerve fiber layer of GK rats only (white arrows). **(B)** Quantification of the VEGF and VEGFR2 immunoreactivity in the retina and choroid of GK rats (n = 8) and age-matched controls (n = 5) based on 12 independent specimen counts *per* eye. VEGF and VEGFR2 immunoreactivities were quantified as fluorescence intensity/area per layer. Counting was done for the right eye only, in all animals. Data are expressed as mean ± SEM. Scale bar: 100 μm. Significance between groups was determined using the independent *t*-test: *$p < 0.05$. GCL, ganglion cell layer; IPL, inner plexiform layer; INL, inner nuclear layer; OPL, outer plexiform layer; ONL, outer nuclear layer; OLM, outer limiting membrane; RPE, retinal pigment epithelium.

flux in diabetes [60]. Anti-VEGFs counteract all these actions. Furthermore, anti-VEGFs counteract the renin-angiotensin-aldosterone system (RAAS) - VEGF crosstalk in the choroid [67], known to have an important role in the increased fluid overload present in the pachychoroid syndromes and primary aldosteronism [68,69]. RAAS components present in retinal cells, in the RPE and the choroid, were shown to be involved in the genesis of DME through the proliferation and activation of glial cells, expressing angiotensin receptor 1, mineralocorticoid receptor and aldosterone synthase. These inflammatory events caused by increased RAAS activity were amplified by the advanced glycation end-products (AGEs), resulting in the release of inflammatory cytokines, leading to leukostasis and apoptosis of retinal pericytes. Furthermore, RAAS may directly impair the water balance of the retina, acting directly on Müller cells, and intravitreal injection of aldosterone causes increased CT and leakage from choroidal vessels [70].

The assumption that the CT is increased in diabetes and that it decreases with anti-VEGFs to a somewhere baseline value is far from being consensual [12]. Moreover, HbA1c levels are known to be correlated with VEGF levels and inflammation [4,71], but high HbA1c levels have been surprisingly correlated with choroidal thinning, and not with the expected choroidal thickening [21]. These contradictions address the need to be cautious when extrapolating the results of our study to human subjects. It would be worth to investigate whether the CT increases in all obese animal models of T2D. Since GK rats are a non-obese model of T2D, one cannot exclude that this particular feature is characteristic of the animal model and not of the disease itself. It is possible that the increased CT found may be constitutive of the animal model, expressing a more vasodilated basal status of the vasoregulatory mechanisms, a feature seen among human subjects as well, expressed by CT inter-individual variability [25]. Therefore, it would be useful that in future studies other animal models of T2D would be used to compare with these results.

Unfortunately, hitherto OCTA does not detect structures with no significant erythrocyte movement, such as the suprachoroid. Therefore, it does not add much in the evaluation of the whole CT [50]. This is why the binarization technique applied to full CT was also applied to EDI OCT, showing no change in CT in diabetes, despite a reduction of the subfoveal choroidal vascular index [72].

5. Conclusions

In conclusion, we found an increase in CT, a decrease in inner choroidal vascular density, increased Iba1$^+$ cells density in the outer retina, and increased VEGFR2 immunoreactivity in the retina, in GK rats. Disposition of pericytes and Iba1$^+$ cells in the choroidal stroma spare the innermost choroid, either in GK or age-matched control Wistar Han rats.

Funding

Declaration of Competing Interest

AC participates in advisory boards for Novartis. RS is a member of the Advisory Boards for Bayer, Alcon, Alimera, Allergan, Novartis, and Thea.

Appendix A. Supplementary data

Supplementary material related to this article can be found, in the online version, at doi:https://doi.org/10.1016/j.biopha.2020.110811.

References

[1] K.M. Bullard, C.C. Cowie, S.E. Lessem, S.H. Saydah, A. Menke, L.S. Geiss, T.J. Orchard, D.B. Rolka, G. Imperatore, Prevalence of diagnosed diabetes in adults by diabetes type - United States, 2016, MMWR Morb. Mortal. Wkly. Rep. 67 (2018) 359–361, https://doi.org/10.15585/mmwr.mm6712a2.

[2] J.G. Gross, A.R. Glassman, D. Liu, J.K. Sun, A.N. Antoszyk, C.W. Baker, N.M. Bressler, M.J. Elman, F.L. Ferris 3rd, T.W. Gardner, L.M. Jampol, D.F. Martin, M. Melia, C.R. Stockdale, R.W. Beck, N. Diabetic Retinopathy Clinical Research, Five-year outcomes of panretinal photocoagulation vs intravitreous ranibizumab for proliferative diabetic retinopathy: a randomized clinical trial, JAMA Ophthalmol. 136 (2018) 1138–1148, https://doi.org/10.1001/jamaophthalmol.2018.3255.

[3] T. Qaum, Q. Xu, A.M. Joussen, M.W. Clemens, W. Qin, K. Miyamoto, H. Hassessian, S.J. Wiegand, J. Rudge, G.D. Yancopoulos, A.P. Adamis, VEGF-initiated blood-retinal barrier breakdown in early diabetes, Invest. Ophthalmol. Vis. Sci. 42 (2001) 2408–2413.

[4] N. Baharivand, N. Zarghami, F. Panahi, M.Y. Dokht Ghafari, A. Mahdavi Fard, A. Mohajeri, Relationship between vitreous and serum vascular endothelial growth factor levels, control of diabetes and microalbuminuria in proliferative diabetic retinopathy, Clin. Ophthalmol. 6 (2012) 185–191, https://doi.org/10.2147/OPTH.S27423.

[5] H.P. Hammes, J. Lin, O. Renner, M. Shani, A. Lundqvist, C. Betsholtz, M. Brownlee, U. Deutsch, Pericytes and the pathogenesis of diabetic retinopathy, Diabetes 51 (2002) 3107–3112, https://doi.org/10.2337/diabetes.51.10.3107.

[6] H. Funatsu, H. Yamashita, T. Ikeda, T. Mimura, S. Eguchi, S. Hori, Vitreous levels of interleukin-6 and vascular endothelial growth factor are related to diabetic macular edema, Ophthalmology 110 (2003) 1690–1696, https://doi.org/10.1016/S0161-6420(03)00568-2.

[7] V.H. Gonzalez, J. Campbell, N.M. Holekamp, S. Kiss, A. Loewenstein, A.J. Augustin, J. Ma, A.C. Ho, V. Patel, S.M. Whitcup, P.U. Dugel, Early and long-term responses to anti-vascular endothelial growth factor therapy in diabetic macular edema: analysis of protocol I data, Am. J. Ophthalmol. 172 (2016) 72–79, https://doi.org/10.1016/j.ajo.2016.09.012.

[8] A. Rubsam, S. Parikh, P.E. Fort, Role of inflammation in diabetic retinopathy, Int. J. Mol. Sci. 19 (2018), https://doi.org/10.3390/ijms19040942.

[9] F.S. Sorrentino, M. Allkabes, G. Salsini, C. Bonifazzi, P. Perri, The importance of glial cells in the homeostasis of the retinal microenvironment and their pivotal role in the course of diabetic retinopathy, Life Sci. 162 (2016) 54–59, https://doi.org/10.1016/j.lfs.2016.08.001.

[10] G.A. Lutty, Effects of diabetes on the eye, Invest. Ophthalmol. Vis. Sci. 54 (2013), https://doi.org/10.1167/iovs.13-12979. ORSF81-87.

[11] A.A. Hidayat, B.S. Fine, Diabetic choroidopathy. Light and electron microscopic observations of seven cases, Ophthalmology 92 (1985) 512–522.

[12] A. Campos, E.J. Campos, J. Martins, A.F. Ambrosio, R. Silva, Viewing the choroid: where we stand, challenges and contradictions in diabetic retinopathy and diabetic macular oedema, Acta Ophthalmol. 95 (2017) 446–459, https://doi.org/10.1111/aos.13210.

[13] H. Endo, S. Kase, M. Takahashi, M. Saito, M. Yokoi, C. Sugawara, S. Katsuta, S. Ishida, M. Kase, Relationship between diabetic macular edema and choroidal layer thickness, PLoS One 15 (2020), e0226630, https://doi.org/10.1371/journal.pone.0226630.

[14] D.M.F. Mohamed, N.A. Hassan, A.A. Osman, M.H. Osman, Subfoveal choroidal thickness in diabetic macular edema, Clin. Ophthalmol. 13 (2019) 921–925, https://doi.org/10.2147/OPTH.S207376.

[15] C. Gupta, R. Tan, C. Mishra, N. Khandelwal, R. Raman, R. Kim, R. Agrawal, P. Sen, Choroidal structural analysis in eyes with diabetic retinopathy and diabetic macular edema—A novel OCT based imaging biomarker, PLoS One 13 (2018), e0207435, https://doi.org/10.1371/journal.pone.0207435.

[16] B. Abadia, I. Suñen, P. Calvo, F. Bartol, G. Verdes, A. Ferreras, Choroidal thickness measured using swept-source optical coherence tomography is reduced in patients with type 2 diabetes, PLoS One 13 (2018), e0191977, https://doi.org/10.1371/journal.pone.0191977.

[17] V. Ambiya, A. Kumar, V.K. Baranwal, G. Kapoor, A. Arora, N. Kalra, J. Sharma, Change in subfoveal choroidal thickness in diabetes and in various grades of diabetic retinopathy, Int. J. Retina Vitreous 4 (2018) 34, https://doi.org/10.1186/s40942-018-0136-9.

[18] A. El Hofi, Corneal endothelial cell changes following Femtosecond laser - assisted cataract surgery versus phacoemulsification, Delta J. Ophthalmol. 19 (2018) 53–57, https://doi.org/10.4103/jcrs.Jcrs_6_19.

[19] K. El Ghonemy, G.Z. Rajab, A.M. Ibrahim, I.M. Gohar, Comparison between choroidal thickness in patients with diabetic retinopathy and normal individuals using enhanced-depth imaging spectral-domain optical coherence tomography, Delta J Ophthalmol. 19 (2018) 53–57. http://www.djo.eg.net/text.asp?2018/19/1/53/224572.

[20] S. Narnaware, P. Bawankule, D. Raje, M. Chakraborty, Choroidal thickness in type 2 diabetic patients with various stages of diabetic macular edema and retinopathy: a prospective study from central India, J. Clin. Ophthalmol. Res. 7 (2019) 12–17, https://doi.org/10.4103/jcor.jcor_124_17.

[21] H. Torabi, M. Saberi Isfeedvajani, M. Ramezani, S.-H. Daryabari, Choroidal thickness and hemoglobin A1c levels in patients with Type 2 diabetes mellitus, J. Ophthalmic Vis. Res. 14 (2019) 285–290, https://doi.org/10.18502/jovr.v14i3.4784.

[22] R. Rewbury, A. Want, R. Varughese, V. Chong, Subfoveal choroidal thickness in patients with diabetic retinopathy and diabetic macular oedema, Eye 30 (2016) 1568–1572, https://doi.org/10.1038/eye.2016.187.

[23] S. Kase, H. Endo, M. Yokoi, M. Kotani, S. Katsuta, M. Takahashi, M. Kase, Choroidal thickness in diabetic retinopathy in relation to long-term systemic treatments for diabetes mellitus, Eur. J. Ophthalmol. 26 (2016) 158–162, https://doi.org/10.5301/ejo.5000676.

[24] W. Wang, S. Liu, Z. Qiu, M. He, L. Wang, Y. Li, W. Huang, Choroidal thickness in diabetes and diabetic retinopathy: a swept source OCT study, Invest. Ophthalmol. Vis. Sci. 61 (2020) 29, https://doi.org/10.1167/iovs.61.4.29.

[25] A. Campos, E.J. Campos, A. do Carmo, M. Patrício, J.P. Castro de Sousa, A.F. Ambrósio, R. Silva, Choroidal thickness changes stratified by outcome in real-world treatment of diabetic macular edema, Graefes Arch. Clin. Exp. Ophthalmol. 256 (2018) 1857–1865, https://doi.org/10.1007/s00417-018-4072-z.

[26] J.L. Federman, The fenestrations of the choriocapillaris in the presence of choroidal melanoma, Trans. Am. Ophthalmol. Soc. 80 (1982) 498–516.

[27] Y. Shimomura, A. Hirata, S. Ishikawa, S. Okinami, Changes in choriocapillaris fenestration of rat eyes after intravitreal bevacizumab injection, Graefes Arch. Clin. Exp. Ophthalmol. 247 (2009) 1089–1094, https://doi.org/10.1007/s00417-009-1054-1.

[28] M. Fukami, T. Iwase, K. Yamamoto, H. Kaneko, S. Yasuda, H. Terasaki, Changes in retinal microcirculation after intravitreal ranibizumab injection in eyes with macular edema secondary to branch retinal vein occlusion, Invest. Ophthalmol. Vis. Sci. 58 (2017) 1246–1255, https://doi.org/10.1167/iovs.16-21115.

[29] M.C. Sabaner, M. Doğan, R. Duman, Effect of intravitreal aflibercept treatment on retinal vessel parameters in diabetic macular oedema: arteriolar vasoconstriction, Cutan. Ocul. Toxicol. 38 (2019) 267–273, https://doi.org/10.1080/15569527.2019.1594875.

[30] D.H. Jo, C.S. Cho, J.H. Kim, H.O. Jun, J.H. Kim, Animal models of diabetic retinopathy: doors to investigate pathogenesis and potential therapeutics, J. Biomed. Sci. 20 (2013) 38, https://doi.org/10.1186/1423-0127-20-38.

[31] A.J.F. King, The use of animal models in diabetes research, Br. J. Pharmacol. 166 (2012) 877–894, https://doi.org/10.1111/j.1476-5381.2012.01911.x.

[32] D.A. Barrière, C. Noll, G. Roussy, F. Lizotte, A. Kessai, K. Kirby, K. Belleville, N. Beaudet, J.-M. Longpré, A.C. Carpentier, P. Geraldes, P. Sarret, Combination of high-fat/high-fructose diet and low-dose streptozotocin to model long-term type-2 diabetes complications, Sci. Rep. 8 (2018) 424, https://doi.org/10.1038/s41598-017-18896-5.

[33] R. Fernandes, A.L. Carvalho, A. Kumagai, R. Seica, K. Hosoya, T. Terasaki, J. Murta, P. Pereira, C. Faro, Downregulation of retinal GLUT1 in diabetes by ubiquitinylation, Mol. Vis. 10 (2004) 618–628.

[34] A. Carmo, J.G. Cunha-Vaz, A.P. Carvalho, M.C. Lopes, Nitric oxide synthase activity in retinas from non-insulin-dependent diabetic Goto-Kakizaki rats: correlation with blood–retinal barrier permeability, Nitric Oxide 4 (2000) 590–596, https://doi.org/10.1006/niox.2000.0312.

[35] S. Omri, F. Behar-Cohen, Y. de Kozak, F. Sennlaub, L.M. Verissimo, L. Jonet, M. Savoldelli, B. Omri, P. Crisanti, Microglia/macrophages migrate through retinal epithelium barrier by a transcellular route in diabetic retinopathy: role of PKCzeta in the Goto Kakizaki rat model, Am. J. Pathol. 179 (2011) 942–953, https://doi.org/10.1016/j.ajpath.2011.04.018.

[36] A. Daruich, A. Matet, A. Moulin, L. Kowalczuk, M. Nicolas, A. Sellam, P.R. Rothschild, S. Omri, E. Gelize, L. Jonet, K. Delaunay, Y. De Kozak, M. Berdugo, M. Zhao, P. Crisanti, F. Behar-Cohen, Mechanisms of macular edema: beyond the surface, Prog. Retin. Eye Res. 63 (2018) 20–68, https://doi.org/10.1016/j.preteyeres.2017.10.006.

[37] D.J. Moore, G.M. Clover, The effect of age on the macromolecular permeability of human Bruch's membrane, Invest. Ophthalmol. Vis. 42 (2001) 2970–2975.

[38] M.R.P. Alves, R. Boia, E.J. Campos, J. Martins, S. Nunes, M.H. Madeira, A.R. Santiago, F.C. Pereira, F. Reis, A.F. Ambrósio, F.I. Baptista, Subtle thinning of retinal layers without overt vascular and inflammatory alterations in a rat model of prediabetes, Mol. Vis. 24 (2018) 353–366.

[39] R.F. Spaide, H. Koizumi, M.C. Pozzoni, Enhanced depth imaging spectral-domain optical coherence tomography, Am. J. Ophthalmol. 146 (2008) 496–500, https://doi.org/10.1016/j.ajo.2008.05.032.

[40] L. Fernandez-Sanchez, L.P. de Sevilla Muller, N.C. Brecha, N. Cuenca, Loss of outer retinal neurons and circuitry alterations in the DBA/2J mouse, Invest. Ophthalmol. Vis. Sci. 55 (2014) 6059–6072, https://doi.org/10.1167/iovs.14-14421.

[41] C.A. Schneider, W.S. Rasband, K.W. Eliceiri, NIH Image to ImageJ: 25 years of image analysis, Nat. Methods 9 (2012) 671–675, https://doi.org/10.1038/nmeth.2089.

[42] A. Kumar, L. Zhao, R.N. Fariss, P.G. McMenamin, W.T. Wong, Vascular associations and dynamic process motility in perivascular myeloid cells of the mouse choroid: implications for function and senescent change, Invest. Ophthalmol. Vis. Sci. 55 (2014) 1787–1796, https://doi.org/10.1167/iovs.13-13522.

[43] B. Portha, M.H. Giroix, C. Tourrel-Cuzin, H. Le-Stunff, J. Movassat, The GK rat: a prototype for the study of non-overweight type 2 diabetes, Methods Mol. Biol. 933 (2012) 125–159, https://doi.org/10.1007/978-1-62703-068-7_9.

[44] P. Sengupta, The laboratory rat: relating its age with human's, Int. J. Prev. Med. 4 (2013) 624–630.

[45] J. Castro-Correia, Understanding the choroid, Int. Ophthalmol. 19 (1995) 135–147.

[46] F.F. Conti, V.L. Qin, E.B. Rodrigues, S. Sharma, A.V. Rachitskaya, J.P. Ehlers, R.P. Singh, Choriocapillaris and retinal vascular plexus density of diabetic eyes using

[47] split-spectrum amplitude decorrelation spectral-domain optical coherence tomography angiography, Br. J. Ophthalmol. 103 (2019) 452–456, https://doi.org/10.1136/bjophthalmol-2018-311903.

[47] I. Gendelman, A.Y. Alibhai, E.M. Moult, E.S. Levine, P.X. Braun, N. Mehta, Y. Zhao, A. Ishibazawa, O.A. Sorour, C.R. Baumal, A.J. Witkin, E. Reichel, J.G. Fujimoto, J.S. Duker, N.K. Waheed, Topographic analysis of macular choriocapillaris flow deficits in diabetic retinopathy using swept-source optical coherence tomography angiography, Int. J. Retina Vitreous 6 (2020) 6, https://doi.org/10.1186/s40942-020-00209-0.

[48] M.F. Abalem, H. Nazareth Veloso Dos Santos, R. Garcia, X.D. Chen, P.C. Carricondo, L. Cabral Zacharias, R.C. Preti, The effect of glycaemia on choroidal thickness in different stages of diabetic retinopathy, Ophthalmic Res. (2020), https://doi.org/10.1159/000506381.

[49] H. Wang, Y. Tao, Choroidal structural changes correlate with severity of diabetic retinopathy in diabetes mellitus, BMC Ophthalmol. 19 (2019) 186, https://doi.org/10.1186/s12886-019-1189-8.

[50] E. Borrelli, D. Sarraf, K.B. Freund, S.R. Sadda, OCT angiography and evaluation of the choroid and choroidal vascular disorders, Prog. Retin. Eye Res. 67 (2018) 30–55, https://doi.org/10.1016/j.preteyeres.2018.07.002.

[51] W. Ma, L. Zhao, A.M. Fontainhas, R.N. Fariss, W.T. Wong, Microglia in the mouse retina alter the structure and function of retinal pigmented epithelial cells: a potential cellular interaction relevant to AMD, PLoS One 4 (2009), e7945, https://doi.org/10.1371/journal.pone.0007945.

[52] A. Campos, E.J. Campos, J. Martins, F.S. Rodrigues, R. Silva, A.F. Ambrósio, Inflammatory cells proliferate in the choroid and retina without choroidal thickness change in early Type 1 diabetes, Exp. Eye Res. (2020), 108195, https://doi.org/10.1016/j.exer.2020.108195.

[53] D. Sun, D. Nakao, F. Xie, S. Zandi, A. Bagheri, M.R. Kanavi, S. Samiei, Z.S. Soheili, S. Frimmel, Z. Zhang, Z. Ablonczy, H. Ahmadieh, A. Hafezi-Moghadam, Molecular imaging reveals elevated VEGFR-2 expression in retinal capillaries in diabetes: a novel biomarker for early diagnosis, FASEB J. 28 (2014) 3942–3951, https://doi.org/10.1096/fj.14-251934.

[54] K. Okabe, S. Kobayashi, T. Yamada, T. Kurihara, I. Tai-Nagara, T. Miyamoto, Y.S. Mukouyama, T.N. Sato, T. Suda, M. Ema, Y. Kubota, Neurons limit angiogenesis by titrating VEGF in retina, Cell 159 (2014) 584–596, https://doi.org/10.1016/j.cell.2014.09.025.

[55] A.B. Condren, A. Kumar, P. Mettu, K.J. Liang, L. Zhao, J.Y. Tsai, R.N. Fariss, W.T. Wong, Perivascular mural cells of the mouse choroid demonstrate morphological diversity that is correlated to vasoregulatory function, PLoS One 8 (2013), e53386, https://doi.org/10.1371/journal.pone.0053386.

[56] R.B. Caldwell, M.E. Fitzgerald, The choriocapillaris in spontaneously diabetic rats, Microvasc. Res. 42 (1991) 229–244, https://doi.org/10.1016/0026-2862(91)90058-j.

[57] T. Baba, R. Grebe, T. Hasegawa, I. Bhutto, C. Merges, D.S. McLeod, G.A. Lutty, Maturation of the Fetal Human Choriocapillaris, Invest. Ophthalmol. Vis. Sci. 50 (2009) 3503–3511, https://doi.org/10.1167/iovs.08-2614.

[58] Z. Chu, G. Gregori, P.J. Rosenfeld, R.K. Wang, Quantification of choriocapillaris with optical coherence tomography angiography: a comparison study, Am. J. Ophthalmol. 208 (2019) 111–123, https://doi.org/10.1016/j.ajo.2019.07.003.

[59] M.E. Langham, R. Grebe, S. Hopkins, S. Marcus, M. Sebag, Choroidal blood flow in diabetic retinopathy, Exp. Eye Res. 52 (1991) 167–173, https://doi.org/10.1016/0014-4835(91)90256-E.

[60] T. Nagaoka, N. Kitaya, R. Sugawara, H. Yokota, F. Mori, T. Hikichi, N. Fujio, A. Yoshida, Alteration of choroidal circulation in the foveal region in patients with type 2 diabetes, Br. J. Ophthalmol. 88 (2004) 1060, https://doi.org/10.1136/bjo.2003.035345.

[61] M. Saint-Geniez, T. Kurihara, E. Sekiyama, A.E. Maldonado, P.A. D'Amore, An essential role for RPE-derived soluble VEGF in the maintenance of the choriocapillaris, Proc. Natl. Acad. Sci. U. S. A. 106 (2009) 18751–18756, https://doi.org/10.1073/pnas.0905010106.

[62] M.A. Fields, L.V. Del Priore, R.A. Adelman, L.J. Rizzolo, Interactions of the choroid, Bruch's membrane, retinal pigment epithelium, and neurosensory retina collaborate to form the outer blood-retinal-barrier, Prog. Retin. Eye Res. 76 (2020), 100803, https://doi.org/10.1016/j.preteyeres.2019.100803.

[63] T. Nishikawa, D. Edelstein, X.L. Du, S.-i. Yamagishi, T. Matsumura, Y. Kaneda, M.A. Yorek, D. Beebe, P.J. Oates, H.-P. Hammes, I. Giardino, M. Brownlee, Normalizing mitochondrial superoxide production blocks three pathways of hyperglycaemic damage, Nature 404 (2000) 787–790, https://doi.org/10.1038/35008121.

[64] A. Campos, E.J. Campos, J. Martins, A.F. Ambrósio, R. Silva, The value of choroidal thickness in diabetic macular oedema is contradictory, Acta Ophthalmol. (2020), https://doi.org/10.1111/aos.14529.

[65] C.-D. Agardh, E. Agardh, H. Zhang, C.-G. Östenson, Altered endothelial/pericyte ratio in Goto-Kakizaki rat retina, J. Diabetes Complicat. 11 (1997) 158–162, https://doi.org/10.1016/S1056-8727(96)00049-9.

[66] D. Fukumura, T. Gohongi, A. Kadambi, Y. Izumi, J. Ang, C.-O. Yun, D.G. Buerk, P.L. Huang, R.K. Jain, Predominant role of endothelial nitric oxide synthase in vascular endothelial growth factor-induced angiogenesis and vascular permeability, Proc. Natl. Acad. Sci. 98 (2001) 2604, https://doi.org/10.1073/pnas.041359198.

[67] S. Simão, D.F. Santos, G.A. Silva, Aliskiren decreases oxidative stress and angiogenic markers in retinal pigment epithelium cells, Angiogenesis 20 (2017) 175–181, https://doi.org/10.1007/s10456-016-9526-5.

[68] M. Zhao, I. Célérier, E. Bousquet, J.-C. Jeanny, L. Jonet, M. Savoldelli, O. Offret, A. Curan, N. Farman, F. Jaisser, F. Behar-Cohen, Mineralocorticoid receptor is

involved in rat and human ocular chorioretinopathy, J. Clin. Invest. 122 (2012) 2672–2679, https://doi.org/10.1172/JCI61427.

[69] E.H.C. van Dijk, M.F. Nijhoff, E.K. de Jong, O.C. Meijer, A.P.J. de Vries, C.J. F. Boon, Central serous chorioretinopathy in primary hyperaldosteronism, Graefes Arch. Clin. Exp. Ophthalmol. 254 (2016) 2033–2042, https://doi.org/10.1007/s00417-016-3417-8.

[70] J.L. Wilkinson-Berka, V. Suphapimol, J.R. Jerome, D. Deliyanti, M.J. Allingham, Angiotensin II and aldosterone in retinal vasculopathy and inflammation, Exp. Eye Res. 187 (2019), 107766, https://doi.org/10.1016/j.exer.2019.107766.

[71] I.M. Stratton, A.I. Adler, H.A.W. Neil, D.R. Matthews, S.E. Manley, C.A. Cull, D. Hadden, R.C. Turner, R.R. Holman, Association of glycaemia with macrovascular and microvascular complications of type 2 diabetes (UKPDS 35): prospective observational study, BMJ 321 (2000) 405, https://doi.org/10.1136/bmj.321.7258.405.

[72] K.A. Tan, A. Laude, V. Yip, E. Loo, E.P. Wong, R. Agrawal, Choroidal vascularity index - a novel optical coherence tomography parameter for disease monitoring in diabetes mellitus? Acta Ophthalmol. 94 (2016) e612–e616, https://doi.org/10.1111/aos.13044.